



RESEARCH ARTICLE

Transient magnesium-based thin-film temperature sensor on a flexible, bioabsorbable substrate for future medical applications

Kevin A. Janus^{1,2}  | Stefan Achtsnicht¹ | Aleksander Drinic³ | Alexander Kopp³ | Michael Keusgen² | Michael J. Schöning^{1,4} 

¹Institute of Nano- and Biotechnologies (INB), FH Aachen, Jülich, Germany

²Institute for Pharmaceutical Chemistry, Philips University of Marburg, Marburg, Germany

³Fibrothelium GmbH, Aachen, Germany

⁴Institute of Biological Information Processing (IBI-3), Forschungszentrum Jülich GmbH, Jülich, Germany

Correspondence

Michael J. Schöning, Institute of Nano- and Biotechnologies (INB), FH Aachen, Campus Jülich, Jülich 52428, Germany.
Email: schoening@fh-aachen.de

Abstract

In this work, the bioabsorbable materials, namely fibroin, polylactide acid (PLA), magnesium, and magnesium oxide are investigated for their application as transient, resistive temperature detectors (RTD). For this purpose, a thin-film magnesium-based meander-like electrode is deposited onto a flexible, bioabsorbable substrate (fibroin or PLA) and encapsulated (passivated) by additional magnesium oxide layers on top and below the magnesium-based electrode. The morphology of different layered RTDs is analyzed by scanning electron microscopy. The sensor performance and lifetime of the RTD is characterized both under ambient atmospheric conditions between 30°C and 43°C, and wet tissue-like conditions with a constant temperature regime of 37°C. The latter triggers the degradation process of the magnesium-based layers. The 3-layers RTDs on a PLA substrate could achieve a lifetime of 8.5 h. These sensors also show the best sensor performance under ambient atmospheric conditions with a mean sensitivity of $0.48 \Omega/^{\circ}\text{C} \pm 0.01 \Omega/^{\circ}\text{C}$.

KEYWORDS

bioabsorbable, polylactide acid, resistive temperature detector, silk fibroin

INTRODUCTION

Monitoring the parameters of internal and complex wounds often requires implantable sensor devices, which need to be extracted after their operational time, to exclude chronic issues and long-term consequences, such as biofouling or foreign body response. [1, 2] These additional surgeries add stress and risk to the patient, and an additional burden to the healthcare system. [3]

For this reason, bioabsorbable sensor devices have become a focal point of modern medical research. Here, the sensor should be completely absorbable by the body after a certain period of time and

composed of bioabsorbable functional materials, which enable direct contact with biological interfaces. [4, 5] In addition, the used materials are not permitted to be toxic or to cause any immunological, physiological or mutagenic effect. [6–10] Typical biocompatible materials for implantable sensors are, for example, gold and platinum as well as polymers such as polyethylene glycol (PEG), polylactide acid (PLA), poly (vinyl alcohol) (PVA), chitosan, and fibroin. [11–19] Being at the same time biodegradable, however, further limits the materials in use. Nonetheless, only very few are considered bioabsorbable and materials further offering suitable properties for application as sensors in all due respects are still highly sought after.

This is an open access article under the terms of the [Creative Commons Attribution-NonCommercial](https://creativecommons.org/licenses/by-nc/4.0/) License, which permits use, distribution and reproduction in any medium, provided the original work is properly cited and is not used for commercial purposes.

© 2023 The Authors. *Applied Research* published by Wiley-VCH GmbH.

Recently, silk-fibroin (prepared from the silk worm *Bombyx mori*) has been suggested as material for green and bioabsorbable electronics. [20, 21] It consists of two protein strands, namely sericin and fibroin. After separation and purification of the biocompatible fibroin from the potentially inflammation-causing sericin, fibroin can be processed into a variety of morphologies, like sponges, gels, powders, scaffolds, membranes, or fibers. [22] Fibroin is often discussed as substrate material for bioabsorbable electronics or an encapsulation to increase the biocompatibility of implantable devices. [22–27] A synthetic, commercially available alternative to fibroin depicts PLA, which is synthesized from starch (e.g., from corn, sugar cane, or potatoes). [28] A reasonable number of biomedical studies deal with PLA as material for medical applications, for example, for tissue engineering, drug carrier systems, cancer therapy, skin and tendon regeneration, orthopaedic and dental devices, surgical tools, and also as substrate material for (bio)sensors. [24, 29–33]

To functionalize these bioabsorbable polymers with metal-type electrodes, gold and platinum are commonly used, even though despite their good biocompatibility for use as biomedical devices, they are not bioabsorbable. [5, 34] In contrast, magnesium (Mg) and most of its alloys and oxides (e.g., MgO) can be classified into bioabsorbable. Mg is an abundant and even the fourth most common metal in humans, offering mechanical properties comparable to cortical bones and showing a fundamental role in metabolic processes, protein synthesis, muscle functions, or bone growth. [35–38] In the human body, Mg dissolves completely without toxic by-products. [39] Therefore, it is being considered a bioabsorbable implant material. [37, 38, 40, 41] The hydrolysis rate of Mg depends on environmental conditions and can be controlled by specific alloying. [42, 43] A number of studies have shown that the Mg alloying system WE43 comprising 4 wt% yttrium and 3 wt% Rare Earths (such as neodymium, cerium, or dysprosium) positively influences mechanical properties and corrosion resistance. [41, 44, 45]

Yet, the hydrolyzability of Mg was used to fabricate a series of bioabsorbable electronic components such as an inductor, capacitor, or resistor on silk fibroin. [46] The electronic components are based on Mg or Silicon as conducting path and MgO as dielectric material, deposited onto a fibroin substrate, and could be dissolved within 10 min. Alloying Mg can enhance the durability of such transient electronics. This way, a Mg-Zn-Ca nanofilm as material for flexible and stretchable electronic components, like MOSFETS (metal-oxide-semiconductor field-effect transistor), capacitors, inductors and diodes, was introduced. [47] Further examples of sensor devices imply a multilayer piezoelectric force sensor made of PLA and Mg, [48] an optical sensor, utilizing Mg plasmonic structures that can be applied on human skin, [49] an implanted Mg electrode as impedance sensor for the detection of gastrointestinal anastomotic leaks, while the degree of hydration for future wound monitoring could be investigated using a Silicon electrode with Mg interconnects. [50, 51] Therefore, Mg shows a potential fit with silk fibroin for the provision of bioabsorbable electronics. As an example, fibroin-coated MgO nanospheres were evaluated as contrast agent for bioimaging applications to study cells under a wide-field fluorescence microscope. [52] Moreover, soluble transistors and mechanical energy harvester were created by combining Mg and fibroin (as well as Zinc oxide and MgO) to develop new classes of thin-film electronics. [53]

The positive temperature coefficient of Mg can be exploited for designing a resistive temperature detector (RTD), which could be used, for example, to monitor the temperature of a healing wound. Wound temperatures represent a crucial parameter during the wound healing process. It has been reported that the wound temperature increases to counteract inflammation, while the temperature may decrease when blood circulation to the wound is blocked. [2]

Recently, a Mg electrode surrounded by a layer of Si_3N_4 and SiO_2 , and encapsulated by Ecoflex was used to create a flexible temperature sensor, having a linear range from 20°C up to 50°C and a stable operation time of 1 day. [54] Although Ecoflex is indicated as bioabsorbable polymer, since deteriorating under industrial compost plant conditions within a few weeks, [54–56] only a few studies considering biomedical applications under physiological conditions exist [57–60]: In these experiments the possibility of hydrolyzing Ecoflex could be shown, however, these studies mainly highlighted the use of Ecoflex for bioabsorbable implants instead of material for sensing devices.

In our work, we focus on the development of a fully bioabsorbable RTD for biomedical applications, utilizing fibroin, and PLA as substrate materials, Mg as meander-type resistor structure and MgO as encapsulation layers. Different sensor setups with different layer arrangements are studied by scanning electron microscopy (SEM) as well as resistance measurements. The sensor performance is characterized in a temperature-controlled chamber between 30°C and 43°C for 56 h, both under ambient atmospheric conditions and in a phosphate buffer solution (PBS)-soaked hydrogel at a constant physiological temperature of 37°C.

EXPERIMENTAL PART

Materials

Glycerol (99.5%), ethanol (99%), disodium hydrogen phosphate dihydrate (analytical grade), and sodium dihydrogen phosphate monohydrate (analytical grade) were purchased from Sigma-Aldrich. The medical grade magnesium alloy WE43MEO was further used as target for physical vapor deposition and provided by the manufacturer (Meotec GmbH), while the magnesium oxide was bought from Evochem Advanced Materials GmbH. Medical grade silk fibroin solution (PureSilk[®]) was provided by the manufacturer (Fibrothelium GmbH) and polylactide acid foil (BoPLA NTSS, 50 µm) was purchased from Pütz GmbH + Co. Folien KG. The hydrogel “Neoheal” was ordered from Kikgel Sp. Z o.o. The temperature characterization experiments were performed in an ibidi stage top incubation system blue line from ibidi GmbH in combination with a universal analog input module (NI9219) from National Instruments or a delphin expert logger from Delphin Technology AG. The platinum-based RTD (Pt100, Nr. 181390) was purchased from Conrad Electronic SE.

Preparation of the silk fibroin membrane

The silk fibroin membrane was prepared under cleanroom conditions at 21°C. The fibroin membrane consisted of a mixture of 2 vol.-eq.

PureSilk® solution (8 wt%), 1 vol.-eq. ethanol (50 vol%) and 1 vol.-eq. triol (3 vol%). Ten milliliters of the mixture was casted into a petri dish and dried on the working bench until complete solidification. The dried membrane was carefully removed from the surface and the brittle edges (0.5 cm) were removed to obtain a flexible, transparent membrane with a diameter of 9 cm and a thickness of around 160 μm . Further details of membrane preparation can be found elsewhere. [5, 23, 24]

Fabrication of the magnesium-based resistive temperature sensor on bioabsorbable substrate

The Mg-based RTD consisted of different layer arrangements of Mg and MgO on top of the bioabsorbable substrate (fibroin or PLA), see Figure 1, top row. Note, the different setups are named according to the number of layers on the bioabsorbable substrate: substrate + Mg = "1-layer system"; substrate + Mg + MgO = "2-layers system"; and substrate + MgO + Mg + MgO = "3-layers system".

The meander-shaped electrode was fabricated by physical vapor deposition using a steel shadow mask in a UNIVEX 250 PVD system from Leybold GmbH. The MgO layers were deposited correspondingly but without the shadow mask. This way, the entire substrate

surface or electrode surface and electrode flanks were covered by MgO (see Figure 1, 2-layers system, and 3-layers system).

The contact pads of the 2-layers system and 3-layers system were covered with adhesive tape during evaporation of the top MgO layer. Each RTD consisted of four contact pads of 2×2 mm (for 4-wire measurement) and a 109.5 mm long meander structure. The layer thickness of the Mg resistor was 200 nm and around 400 nm for the MgO protective layers. The substrates had a thickness of 160 μm (fibroin) and 50 μm (PLA). Figure 1 (middle, bottom) depicts top-view microscopic images of the different layer arrangements after fabrication.

Measurement protocol for the characterization of magnesium-based RTDs under ambient atmospheric conditions

The characterization of the Mg-based RTDs under ambient atmospheric conditions was performed in an ibidi-chamber (Figure 2, yellow) and recorded with a NI (National instrument) card or Delphine data logger.

The resistors (one example marked in Figure 2 as green box) were connected in a 4-wire configuration to the measuring devices via a zero insertion force connector (ZIF, Bürklin GmbH & Co KG); see

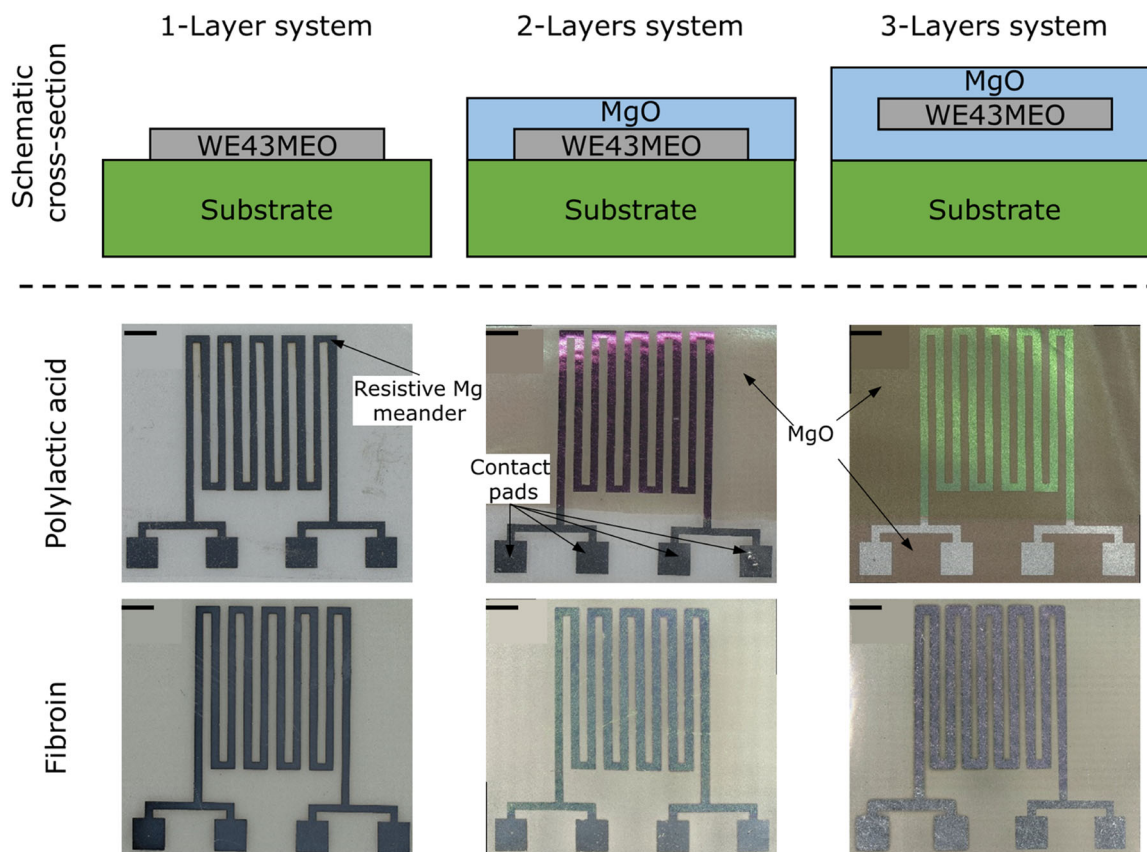


FIGURE 1 Top: schematic cross section (not to scale) of magnesium-based resistive temperature detector (RTD) with different layers of magnesium (WE43MEO) and magnesium oxide (MgO) on bioabsorbable substrates from silk fibroin and polylactide acid. Middle and bottom: microscopic images of the different layer systems for magnesium-based RTDs on the substrates PLA and fibroin. The black scale bar equals 2 mm.

Figure 2 (one example marked in red). The RTDs (up to six sensors) were mounted on a self-constructed 3D-printed sample holder (Figure 2, gray) in the ibidi-chamber, including an additional platinum temperature sensor (Pt100) for reference (blue box).

The sensor characterization was done by recording the resistance over time for 56 h with dynamic temperature variations between 30°C and 42.9°C (in 0.3°C steps every 10 min). This range includes the body's core and extremity temperatures as well as temperatures considered pathological or even lethal. One temperature cycle (from lowest to highest temperature and vice versa) took around 14 h.

Measurement protocol for the characterization of magnesium-based RTDs under tissue-like conditions

The characterization of the Mg-based RTDs under tissue-like conditions was also performed in the climate chamber (Figure 3). Here, the sensors were placed between two hydrogel layers in

contact with a phosphate buffer reservoir below. The temperature was kept constant at 37°C, monitoring the resistance over time. For this experiment, the ibidi-chamber was modified by a self-designed 3D-sample holder consisting of a 3D-printed phosphate buffer reservoir (Figure 3, yellow) with an external tube connector (Figure 3, gray) for refilling, and a 3D-printed cage-like sample holder to keep the sensor and hydrogel in place (Figure 3, blue). The cage-like structure of the sample holder allowed the hydrogel to remain hydrated throughout the experiment.

RESULTS AND DISCUSSION

Scanning electron microscopy analysis of the magnesium-based RTDs on bioabsorbable substrates

The thin-film Mg-based RTDs on bioabsorbable substrates of silk fibroin and PLA, with different layer arrangements, were characterized by

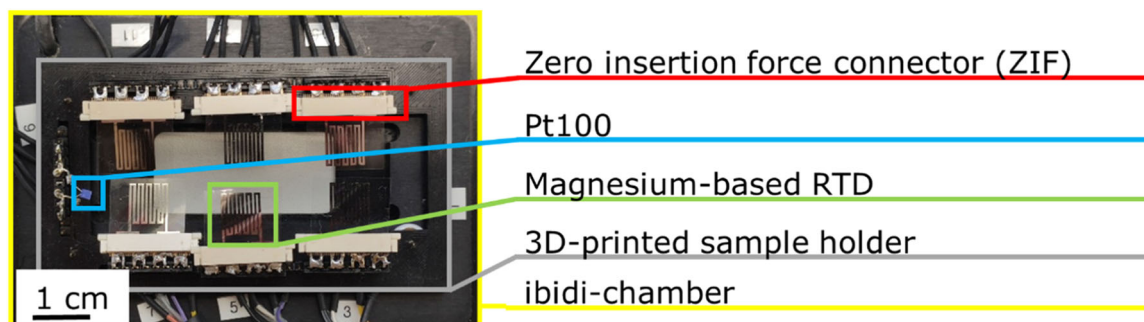


FIGURE 2 Opened climate chamber for magnesium-based RTD characterization under ambient atmospheric conditions. A 3D-printed sample holder (gray) is placed on top of the heated plate (yellow) of the ibidi-chamber to fix the ZIF-connectors in position. The ZIF-connectors (red) connect the magnesium-based RTDs (green) with the measuring device (not shown). Furthermore, a commercial Pt100 (blue) serves as a reference temperature sensor.

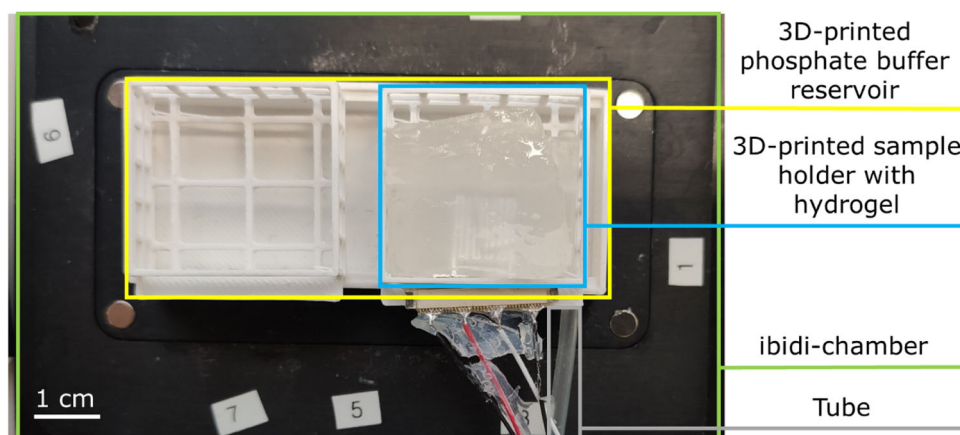


FIGURE 3 Opened climate chamber for magnesium-based RTD characterization under tissue-like conditions. The heated plate (green) of the ibidi-chamber was modified by a 3D-printed phosphate buffer reservoir (yellow) connected to a syringe (not shown) via a flexible tube (gray) to refill the reservoir during experiments. A cage-like 3D-printed sample holder (blue) was placed on top of the phosphate buffer reservoir. Inside this cage are two layers of hydrogel with the magnesium-based RTD in between. The cage-like structure allows direct contact between the hydrogel and the phosphate buffer solution, so that the hydrogel remains hydrated during the experiment.

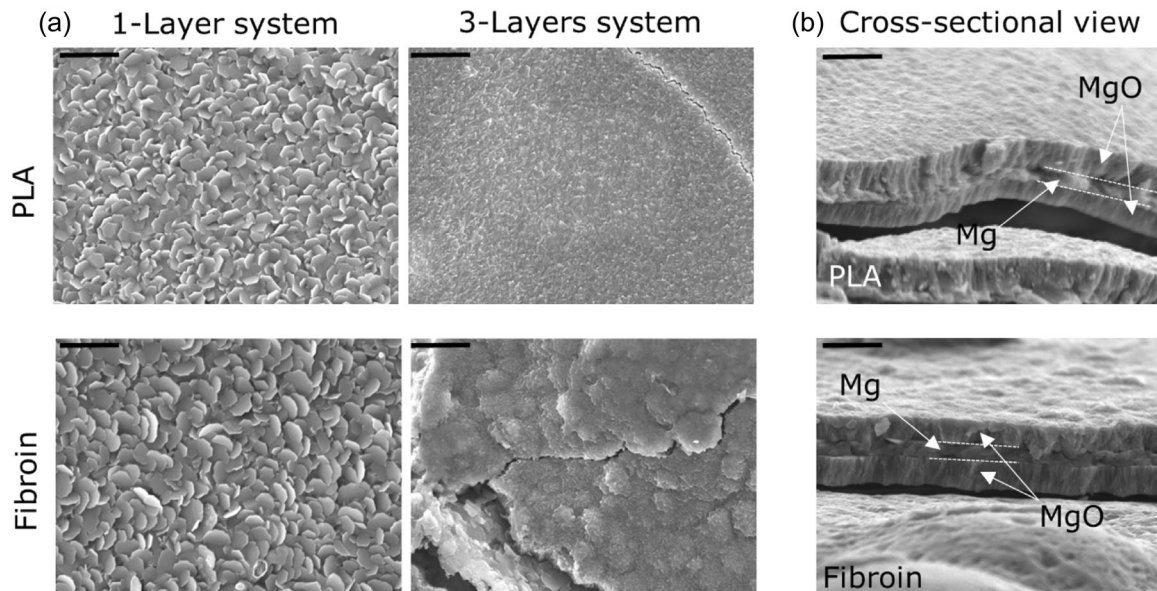


FIGURE 4 SEM images of the different layer systems on PLA (top) and silk fibroin (bottom) in (a) top view on 1-layer system (left) and 3-layers system (middle), and (b) cross-sectional view (right) of the 3-layers system on PLA and fibroin, respectively. The black scale bar indicates 1 μm . Mg, WE43MEO alloy; MgO, magnesium oxide; PLA, polylactide acid.

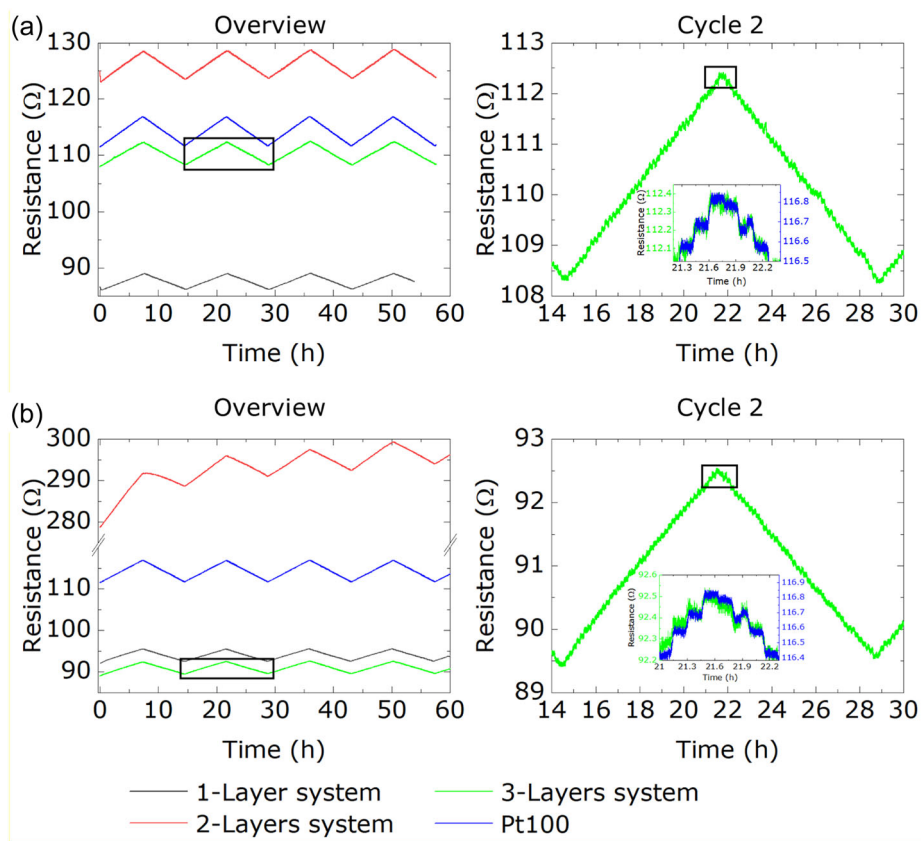


FIGURE 5 Resistance over time measurements for magnesium-based RTDs with different layer systems (black: 1-layer system; red: 2-layers system; green: 3-layers system; blue: Pt100) on bioabsorbable substrates PLA (a) and silk fibroin (b) between 30°C and 42.9°C in 0.3°C steps under ambient atmospheric conditions. The left column overviews the measurement over four cycles (56 h), whereas the right column shows a magnification of the second cycle (from hour 14 to 28) of the 3-layers system. The insets give an exemplary detailed view on the 0.3°C temperature steps of the 3-layers system and the reference Pt100 signal, with axes matching the color. The magnification areas are depicted by black rectangles.

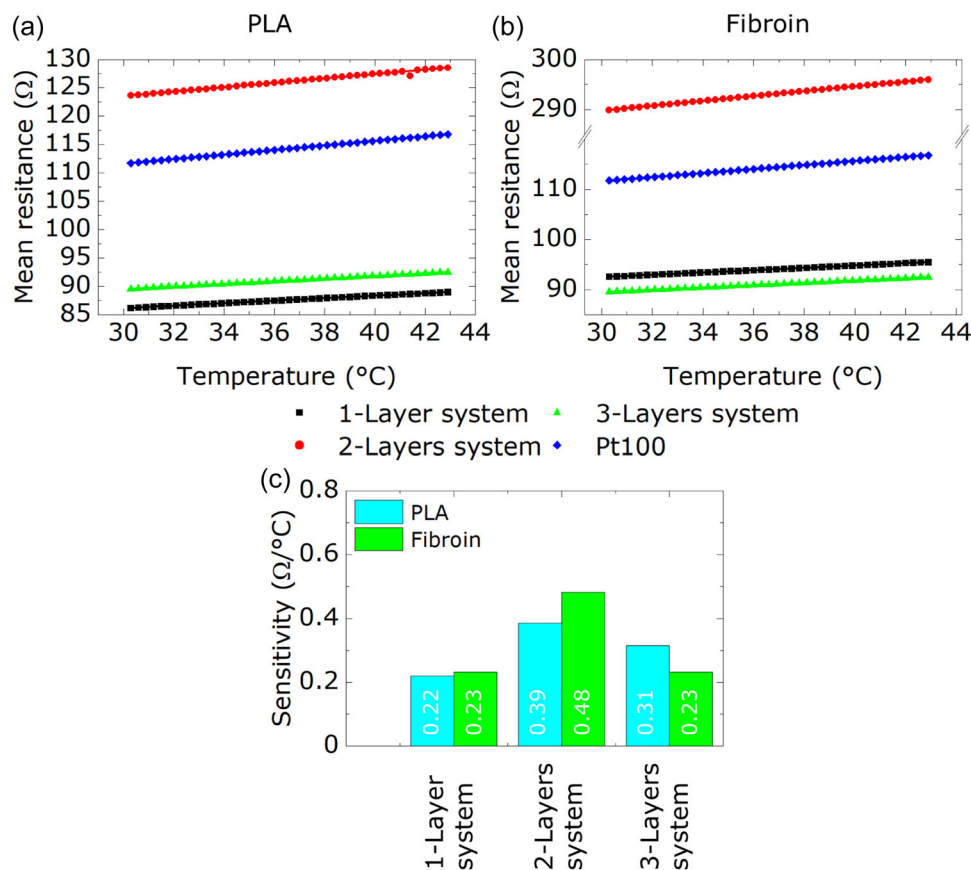


FIGURE 6 Calibration plot for magnesium-based RTDs with different layer systems on the bioabsorbable substrate PLA (a) and fibroin (b) for cycle 2 under ambient atmospheric conditions between 30.3°C and 42.9°C in 0.3°C steps. The data display the mean value for each temperature step from the heating and cooling part of the second cycle. (c) Sensitivity values for the RTDs on PLA (cyan) and silk fibroin (green) obtained from a linear fit between 30.3°C and 42.9°C.

scanning electron microscopy (SEM, JEOL, JSM-7800F) with an applied acceleration voltage of 5.0 kV. The SEM images in Figure 4 address the top view (a) and the cross-sectional view (b) of the different layer systems on PLA (first row) and fibroin (second row).

The top-view images reveal a distinct, scaly-type morphology of the RTD surface on both substrates. For the 1-layer system (Figure 4, left), a grain size diameter of about 500 nm was found (more pronounced for fibroin as substrate material), while the additional MgO layers for the 3-layers systems result in a much smoother RTD surface without any clear fragmentation into single grains (Figure 4, middle). On the other hand, the 3-layers system, deposited onto fibroin shows individual, broken areas, which might increase the subsequent sensor degradation rapidly (see, also Section Characterization of magnesium-based RTDs on bioabsorbable substrates under tissue-like conditions). A similar flake-like morphology for deposited Mg layers as well as a grain-size dependency on the layer thickness was already discussed by other researchers, for example. [61]

The cross-sectional view of the 3-layers system utilizing PLA and silk fibroin, respectively, is exemplarily presented in Figure 4 (right). The images reveal the layer sequence of PLA/MgO (400 nm)/Mg (200 nm)/MgO (440 nm) and fibroin/MgO (460 nm)/Mg (210 nm)/MgO (400 nm), representing typical layer thicknesses in this experiment.

Characterization of magnesium-based RTDs on bioabsorbable substrates under ambient atmospheric conditions

The Mg-based RTDs were studied under ambient atmospheric conditions by recording the resistance over time for repeated heating (up to 42.9°C) and cooling (down to 30°C) steps over at least four cycles for 56 h with the two substrates PLA and silk fibroin (see Figure 5); to be noted, measurements over several weeks were also possible utilizing these sensor chips (data not shown). At least three sensors were studied for each layer system. Considering a layer thickness of the Mg resistor of 200 nm (see, Section Fabrication of the magnesium-based resistive temperature sensor on bioabsorbable substrate) and a temperature coefficient $\alpha = 0.003 \text{ K}^{-1}$ for Mg, [62, 63] the typically achieved RTD values of around 110 Ω at 30°C correspond well with calculated theoretical values of 160 Ω, taking into account that here an alloy is used and not pure Mg. Slight variations of absolute RTD values might be explained due to thickness variations and irregularities within the substrate layer (PLA, silk fibroin), which can lead to thickness deviations in the deposited meander structures.

Figure 5 (left) exhibits exemplary measurement curves for the RTDs with PLA (a) and fibroin (b) as substrate material. In addition,

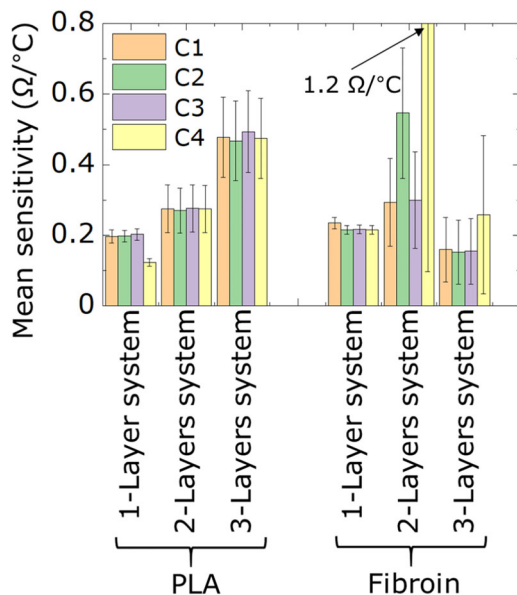


FIGURE 7 Mean sensitivity values and standard deviations of all measured magnesium-based RTDs with different layer systems on the bioabsorbable substrates PLA (left) and fibroin (right) for four cycles (C1, C2, C3, C4). For a better comparison, the graph is set to a maximum mean sensitivity of 0.8 Ω/°C. The value of the 2-layers system on fibroin in cycle 4 is 1.20 ± 1.11 Ω/°C. N(PLA, 1-layer system) = 3, N(PLA, 2-layers system) = 5, N(PLA, 3-layers system) = 6, N(fibroin, 1-layer system) = 3, N(fibroin, 2-layers system) = 3 and N(fibroin, 3-layers system) = 3.

the resistance of the Pt100 as a reference sensor was recorded, too. All RTDs had nearly identical sensor characteristic with increasing/decreasing the temperature in the measurement cycles. Figure 5 (right) shows a magnification of the 3-layers system in cycle 2 with a further zoom into the highest four temperature steps (42.0°C, 42.3°C, 42.6°C, 42.9°C) as inlet. Here, in both cases (RTD with PLA [a], RTD with silk fibroin [b]), the data reveal distinguishable 0.3°C temperature steps. The noisy, wavelike pattern of the sensor signal can be related to the temperature control of the climate chamber itself. Similar signal behavior was also recorded for the Pt100 reference sensor (data not shown). The hysteresis between the heating and cooling part of cycle 2 for the 3-layers system on fibroin is 0.12 Ω at 35.7°C (highest value) and 0.01 Ω at 32.4°C (lowest value), RTDs on PLA display the highest hysteresis values at 34.5°C and 35.1°C with 0.75 and 0.16 Ω, respectively, and the lowest value with 0.01 Ω at 36.6°C. A comparable hysteresis value of 0.77 Ω at 34.5°C was also recorded by the Pt100 reference sensor of class B accuracy (which was running parallel to the 3-layers RTDs on PLA), indicating the fluctuations and deviations in the climate chamber's automated temperature control. Otherwise, the hysteresis of the Pt100 sensor was always within the specification of its accuracy class (class B).

The mean resistance value per temperature step is calculated for cycle 2 as an example and the trend of these values is visualized by means of linear regression in Figure 6a,b. All sensors, regardless of

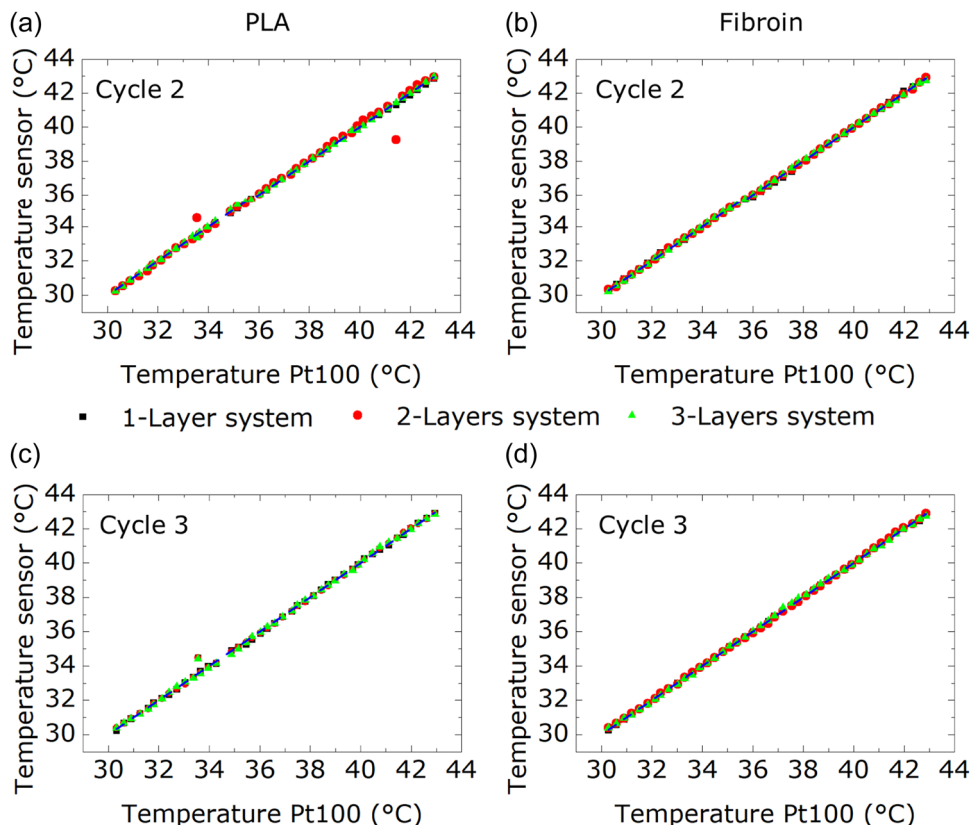


FIGURE 8 Comparative temperature data of magnesium-based RTDs with different layer systems on PLA (a) + (c), and fibroin (b) + (d) with measured temperature values of the Pt100 reference sensor of cycle 2 (top) and cycle 3 (bottom). The blue dotted line marks the diagonal line.



FIGURE 9 Dyeing a piece of hydrogel with cresyl-blue staining solution for 3 h (top row). The piece of hydrogel was cut in half to prove the uniformly stained cross section. Bleaching of the hydrogel by using deionized water (bottom row). After 42 h, no visible sign of the stain remained. The scale bar equals 2 mm.

the studied layer system, show a linear correlation between the mean resistance and temperature. Figure 6c compares the resulting sensitivities: RTDs on both substrates using the 2-layer system display the highest sensitivity values with $0.39 \Omega/^\circ\text{C}$ (PLA as substrate) or $0.48 \Omega/^\circ\text{C}$ (silk fibroin as substrate).

Figure 7 summarizes the mean RTD sensitivities of all measured sensor types (on PLA [left] and silk fibroin [right]) for each layer arrangement (1-layer system, 2-layers system, 3-layers system) for cycle 1 to cycle 4 (C1, C2, C3, C4). The mean sensitivity values for RTDs on PLA, independently of the studied layer system, remain constant over all four measurement cycles. With increasing layer number, the mean sensitivity increased from $0.18 \Omega/^\circ\text{C} \pm 0.03 \Omega/^\circ\text{C}$ to $0.27 \Omega/^\circ\text{C} \pm 0.01 \Omega/^\circ\text{C}$ and $0.48 \Omega/^\circ\text{C} \pm 0.01 \Omega/^\circ\text{C}$ for the 1-layer, 2-layers, and 3-layers system. One possible explanation for this behavior might be an occurring thermal annealing effect of the Mg electrode layer during the deposition process of the top MgO layers. Annealing of Mg can improve its conductivity, but also other properties, like hardness and thermal conductivity, can be influenced by the annealing process. [64, 65]

In contrast, the sensitivity of RTDs on bioabsorbable silk fibroin exhibited pronounced fluctuations, especially for the 2-layers system. The mean sensitivities are $0.22 \Omega/^\circ\text{C} \pm 0.01 \Omega/^\circ\text{C}$ (1-layer system), $0.59 \Omega/^\circ\text{C} \pm 0.43 \Omega/^\circ\text{C}$ (2-layers system) and $0.18 \Omega/^\circ\text{C} \pm 0.05 \Omega/^\circ\text{C}$ (3-layers system). Variations are probably induced by the strong swelling behavior of silk fibroin. [24] For example, the used fibroin composition can absorb up to 50% of its own weight in aqueous solutions. Therefore, it can be assumed that fibroin will shrink significantly under high vacuum during the evaporation process of the electrode/encapsulation material. This could finally result in damaging the Mg electrode during the rehydration process, which will negatively influence the sensor performance. Small cracks in the MgO surface can be observed in the SEM image in Section Scanning electron microscopy analysis of the magnesium-based RTDs on bioabsorbable substrates, Figure 4.

To assign the RTD values to the actual temperature, all sensors were calibrated to the first measurement cycle, according to the following equation:

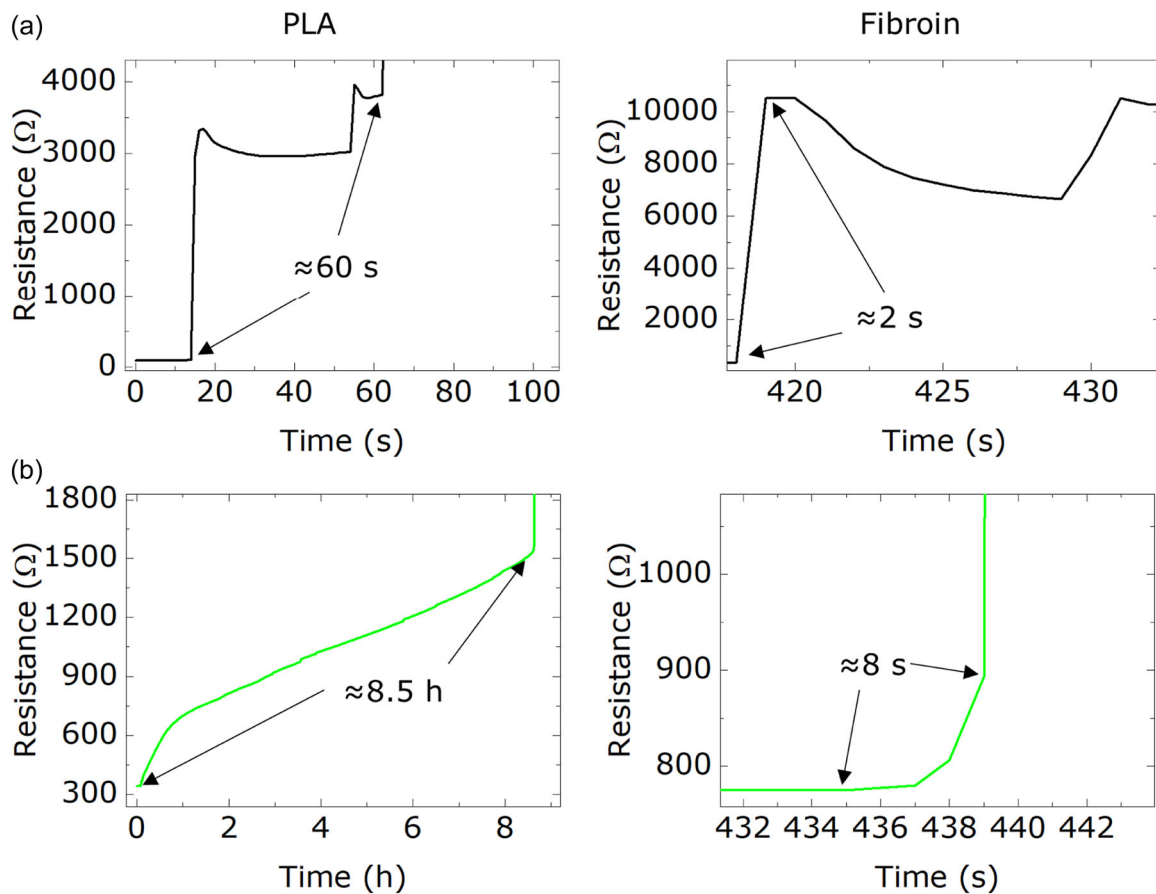


FIGURE 10 Exemplary time-dependent resistance characteristics of magnesium-based RTDs on PLA (left) and fibroin (right) in tissue-like environment at constant temperature of 37°C. (a) 1-layer system, (b) 3-layers system. The sensor operation time is calculated between the addition of the first hydrogel layer and the moment of abrupt resistance rise.

$$R(T) = R_{T_0} [1 + \alpha_{T_0} \times (T - T_0)], \quad (1)$$

with $R(T)$: temperature-dependent resistance [Ω], R_{T_0} : electrical nominal resistance at T_0 (here, 0°C) [Ω], α_{T_0} : linear temperature coefficient at T_0 [$1/K$] ($0.003 K^{-1}$), T : Temperature [$^{\circ}C$] and T_0 reference temperature [$^{\circ}C$], here 0°C.

In Figure 8, the converted temperature data is plotted against values of the reference Pt100 (class B) for the second and third cycle for all RTDs. The blue dashed line visualizes the corresponding diagonal match between the measured RTD values and reference values of the Pt100. Regardless of the studied layer system, all sensors (on both PLA and fibroin) coincided the diagonal line. This behavior was observed for all measurement cycles. For all studied sensors ($N = 18$) in this experiment, there has been a slight variation (i.e., typical for thin-film resistors) of the α values with $\alpha = 0.0029 K^{-1} \pm 0.00024 K^{-1}$.

In summary, it can be concluded that Mg-based RTDs on bioabsorbable substrates are capable of monitoring temperature under ambient atmospheric conditions, independently of the chosen layer setup. PLA-based sensors could easily operate within the period of study (56 h). Fibroin-based sensors exhibited similar RTD characteristics, however, especially the 2-layers system was subject

to fluctuations and inferior stability when compared to the PLA counterparts.

Characterization of magnesium-based RTDs on bioabsorbable substrates under tissue-like conditions

Temperature monitoring after a surgery (to exclude e.g., inflammatory reactions) presumes a bioabsorbable RTD which can be applied in vivo. Here, the sensors meet new challenges, like mechanical stress by movement or pressure of the surrounding tissue, which can influence the measurement results. In addition, under tissue-like conditions the biodegradation of the sensor is triggered by two superposed mechanisms: (i) the substrate can be degraded by enzymes in the human body (e.g., fibroin by protease), causing the sensor to lose its structural integrity [4]; (ii) on the other hand, the humid environment of the tissue leads to hydrolysis of the meander-type resistor structure itself. Comparing these two steps showed that the hydrolysis of the Mg resistor is much faster than the degradation of fibroin or PLA. Mg degradation can occur within a few hours (depending on the layer thickness and the presence of protective layers, see e.g., [42]),

while degradation of fibroin or PLA requires at least several days under optimal enzymatic conditions. [30, 66]

To mimic the scenario of an implantable RTD after surgery, the sensors were tested under tissue-like conditions: for the experimental set-up, two layers of hydrogel were used, where the particular RTD was positioned in between. The hydrogel was synthesized in ultrapure water and exposed to PBS pH 7.4 for 24 h before measurement. The loading/unloading of the hydrogel was previously tested using a stained PBS solution, see Figure 9, demonstrating a good and homogeneous exchange (coloring/bleaching) within 3 h.

The Mg-based RTDs were characterized at 37°C in the modified climate chamber (see, also Figure 3). The operational time of the RTDs was evaluated between the addition of the first layer of hydrogel and that moment of measurement where the resistance increased drastically, as exemplarily indicated in Figure 10. Regardless of the layer system chosen, RTDs on a PLA substrate always have a significantly longer operational time than those on the fibroin substrate. Furthermore, the lifetime of RTDs on both substrates (PLA, silk fibroin) increases with increasing number of layers. The shorter lifetime of the silk fibroin-based RTDs can be explained by the water uptake, [24] which leads to an expansion of the fibroin membrane that possibly mechanically damages the deposited MgO layer. Cracks would result in a shortcut in the aqueous environment to hydrolyze the Mg-based electrode. Furthermore, some water is always bound within the polymer network of the fibroin membrane, which also continuously degrades the resistance structure. PLA will presumably exhibit the same mechanisms, but in a much weaker form, as this material swells less strongly.

An additional layer of MgO on top of the Mg resistor on PLA (2-layers system) increased the operational time from about 60 s to about 350 s (data not shown), and a further protective layer of MgO—inserted between the electrode and the substrate (3-layers system)—yielded a significant increase in lifetime to approx. 8.5 h. In the case of RTDs on the silk fibroin substrate, the different layer systems only slightly enhanced the operational time of the sensor from originally about 2 s to about 8 s.

In summary, the operational time of bioabsorbable Mg-based RTDs can be improved by adding MgO layers on top and below the transient Mg-based resistor layer. The experiments revealed a strong impact of the chosen substrate material to the resulting operational time: Mg-based electrodes on a strongly swelling substrate, such as fibroin, have an exceptionally short lifetime, whereas swelling substrates, such as PLA, allowed monitoring of RTD values up to 8.5 h.

CONCLUSIONS

Bioabsorbable, Mg-based resistive temperature sensors with MgO protective layers were fabricated on flexible and bioabsorbable substrates (PLA and silk fibroin), using thin-film technology. The application of a shadow-mask process can avoid the use of harmful, nonbiocompatible chemicals, typically used in

photolithographic processes. The resulting sensors were characterized under ambient atmospheric conditions ranging between 30°C and 43°C, covering the body's core and extremity temperatures, as well as temperatures considered as pathological or even lethal. All studied sensor systems (1-layer system, 2-layers system, 3-layers system) could be measured for at least 56 h, independently of the selected substrate.

Moreover, the influence of MgO protective layers to the resulting operational time of the resistor was examined under tissue-like conditions. For this reason, the sensor was placed between two layers of a phosphate buffer solution-soaked hydrogel. It could be observed, that a strong-swelling substrate, like silk fibroin, drastically reduces the operational time (in the range of seconds), compared to a less-swelling substrate such as PLA (with lifetime in the order of several hours). In all experiments, the degradation of the electrode was successfully induced. As the sensors were positioned within the hydrogel stack, their resistance steadily increased over time, that is signal changes due to a temperature increase or decrease are superimposed by the drift-based signal change.

To counteract this behavior, next steps might focus on optimizing the substrate properties or targeting the protective layers. Water permeability of silk fibroin or PLA should be reduced by selecting additives. Thicker protective layers could increase the lifetime, but might carry the risk of brittle sensor structures. Alternative biocompatible and bioabsorbable materials should be studied, too. In particular, hydrophobic materials such as a carbon layer or wax could significantly delay the biodegradation of the Mg resistor. Nonetheless, the presented work highlights PLA, silk fibroin, Mg and MgO as suitable “building blocks” for bioabsorbable sensors. Their versatile properties make them an excellent choice for future implantable and transient sensor devices. However, their application is not limited to the medical sector. In particular, the bio-based, renewable nature of PLA and silk-fibroin make them an interesting alternative substrate to replace conventional fuel-based plastics. The proposed sensor systems might also be used for environmental surveillance or even replace nonrecyclable disposable thermometers, thus supporting a future circular economy.

ACKNOWLEDGMENTS

The authors thank D. Rolka for assistance with the SEM images, H. Iken for assistance during electrode fabrication and C. Niebuhr for support with sensor characterization.

CONFLICT OF INTEREST STATEMENT

The authors declare no conflict of interest.

DATA AVAILABILITY STATEMENT

The data that support the findings of this study are available from the corresponding author upon reasonable request.

ORCID

Kevin A. Janus  <http://orcid.org/0000-0001-6056-5941>

Michael J. Schöning  <http://orcid.org/0000-0003-4347-6685>

REFERENCES

- [1] Y. Wang, S. Vaddiraju, B. Gu, F. Papadimitrakopoulos, D. J. Burgess, *J. Diabetes Sci. Technol.* **2015**, *9*, 966.
- [2] D. Özsoylu, K. A. Janus, S. Achtsnicht, T. Wagner, M. Keusgen, M. J. Schöning, *Sens. Actuators Rep.* **2023**, *6*, 100163.
- [3] F. Arab Hassani, Q. Shi, F. Wen, T. He, A. Haroun, Y. Yang, Y. Feng, C. Lee, *Smart Mater. Med.* **2020**, *1*, 92.
- [4] D. Zhang, X. Wu, J. Chen, K. Lin, *Bioact. Mater.* **2018**, *3*, 129.
- [5] D. Molinnus, A. Drinic, H. Iken, N. Kröger, M. Zinser, R. Smeets, M. Köpf, A. Kopp, M. J. Schöning, *Biosens. Bioelectron.* **2021**, *183*, 113204.
- [6] M. Chraniuk, M. Panasiuk, L. Hovhannissyan, S. Żołędowska, D. Nidzworski, L. Ciołek, A. Woźniak, A. Kubiś, N. Karska, Z. Jaegermann, S. Rodziewicz-Motowidło, M. Biernat, B. Gromadzka, *Toxics* **2022**, *10*, 20.
- [7] E. Mariani, G. Lisignoli, R. M. Borzi, L. Pulsatelli, *Int. J. Mol. Sci.* **2019**, *20*, 636.
- [8] S. Al-Maawi, A. Orłowska, R. Sader, C. James Kirkpatrick, S. Ghanaati, *Semin. Immunol.* **2017**, *29*, 49.
- [9] V. J. Cvetković, D. T. Miladinov, S. Stojanović, *Biomaterials in Clinical Practice: Advances in Clinical Research and Medical Devices*, Springer International Publishing, **2018**, pp. 501.
- [10] N. Ashammakhi, A. L. Hernandez, B. D. Unluturk, S. A. Quintero, N. R. de Barros, E. H. Apu, A. Bin Shams, S. Ostrovidov, J. Li, C. Contag, A. S. Gomes, M. Holgado, *Adv. Funct. Mater.* **2021**, *31*, 2104149.
- [11] C. Kojima, H. Xia, Y. Yamamoto, H. Shiigi, *Chem. Nano. Mat.* **2022**, *8*, e202100442.
- [12] J. J. Kim, G. R. Stafford, C. Beauchamp, S. A. Kim, *Sensors* **2020**, *20*, 3953.
- [13] U. Izhar, L. Piyathilaka, D. M. G. Preethichandra, *Neurosci. Informatic.* **2022**, *2*, 100106.
- [14] J. E. Oliveira, L. H. C. Mattoso, E. S. Medeiros, V. Zucolotto, *Biosensors* **2012**, *2*, 70.
- [15] H. Tao, S.-W. Hwang, B. Marelli, B. An, J. E. Moreau, M. Yang, M. A. Brenckle, S. Kim, D. L. Kaplan, J. A. Rogers, F. G. Omenetto, *Proc. Natl. Acad. Sci.* **2014**, *111*, 17385.
- [16] Y. Yun, Z. Dong, N. Lee, Y. Liu, D. Xue, X. Guo, J. Kuhlmann, A. Doepke, H. B. Halsall, W. Heineman, S. Sundaramurthy, M. J. Schulz, Z. Yin, V. Shanov, D. Hurd, P. Nagy, W. Li, C. Fox, *Mater. Today* **2009**, *12*, 22.
- [17] M. Teodorescu, M. Bercea, S. Morariu, *Biotechnol. Adv.* **2019**, *37*, 109.
- [18] P. Ratanasongtham, L. Shank, J. Jakmunee, R. Watanesk, S. Watanesk, *Chiang Mai J. Sci.* **2016**, *50*, 1431.
- [19] S. Qasim, M. Zafar, S. Najeed, Z. Khurshid, A. Shah, S. Husain, I. Rehman, *Int. J. Mol. Sci.* **2018**, *19*, 407.
- [20] C. Lee, S. Kim, Y.-H. Cho, *Adv. Sustain. Syst.* **2022**, *6*, 2000216.
- [21] K. Wang, Q. Ma, H.-T. Zhou, J.-M. Zhao, M. Cao, S.-D. Wang, *Autex Res. J.* **2023**, *23*, 164.
- [22] D.-L. Wen, D.-H. Sun, P. Huang, W. Huang, M. Su, Y. Wang, M.-D. Han, B. Kim, J. Brugger, H.-X. Zhang, X.-S. Zhang, *Microsys. Nanoeng.* **2021**, *7*, 35.
- [23] D. Molinnus, K. A. Janus, A. C. Fang, A. Drinic, S. Achtsnicht, M. Köpf, M. Keusgen, M. J. Schöning, *Phys. Status Solidi* **2022**, *219*, 2200100.
- [24] K. A. Janus, S. Achtsnicht, L. Tempel, A. Drinic, A. Kopp, M. Keusgen, M. J. Schöning, *Phys. Status Solidi* **2023**, *220*, 2300081.
- [25] Z. Wang, H. Yu, Z. Zhao, *Microchem. J.* **2021**, *169*, 106585.
- [26] J. H. Choi, M. Choi, T. S. Ho, S. Kim, S. Choi, S. H. Choi, K. M. Byun, *Opt. Express* **2022**, *30*, 7782.
- [27] J.-H. Liu, W.-D. Li, J. Jia, C.-Y. Tang, S. Wang, P. Yu, Z.-M. Zhang, K. Ke, R.-Y. Bao, Z.-Y. Liu, Y. Wang, K. Zhang, M.-B. Yang, W. Yang, *Nano Energy* **2022**, *103*, 107787.
- [28] A. P. Gupta, V. Kumar, *Eur. Polym. J.* **2007**, *43*, 4053.
- [29] V. DeStefano, S. Khan, A. Tabada, *Eng. Reg.* **2020**, *1*, 76.
- [30] D. Da Silva, M. Kaduri, M. Poley, O. Adir, N. Krinsky, J. Shainsky-Roitman, A. Schroeder, *Chem. Eng. J.* **2018**, *340*, 9.
- [31] S. Pérez-Davila, L. González-Rodríguez, R. Lama, M. López-Álvarez, A. L. Oliveira, J. Serra, B. Novoa, A. Figueras, P. González, *Polymers* **2022**, *14*, 4117.
- [32] L. Ranakoti, B. Gangil, P. Bhandari, T. Singh, S. Sharma, J. Singh, S. Singh, *Molecules* **2023**, *28*, 485.
- [33] X. Ma, Q. Hu, Y. Dai, P. He, X. Zhang, *Sens. Actuators, A* **2022**, *346*, 113834.
- [34] Y. Cui, F. Zhang, G. Chen, L. Yao, N. Zhang, Z. Liu, Q. Li, F. Zhang, Z. Cui, K. Zhang, P. Li, Y. Cheng, S. Zhang, X. Chen, *Adv. Mater.* **2021**, *33*, 2100221.
- [35] M. De Santis, I. Cacciotti, *Nanotechnology* **2020**, *31*, 252001.
- [36] A. M. Al Alawi, S. W. Majoni, H. Falhammar, *Inter. J. Endocrinol* **2018**, *2018*, 9041694.
- [37] I. Marco, A. Myrissa, E. Martinelli, F. Feyerabend, R. Willumeit-Römer, A. Weinberg, van der O. Biest, *Eur. Cells Mater.* **2017**, *33*, 90.
- [38] A. Ferrández-Montero, A. Eguluz, E. Vazquez, J. D. Guerrero, Z. Gonzalez, A. J. Sanchez-Herencia, B. Ferrari, *Polymers* **2021**, *13*, 1061.
- [39] J.-M. Seitz, R. Eifler, F.-W. Bach, H. J. Maier, *J. Biomed. Mater. Res. A.* **2014**, *102*, 3744.
- [40] E. Hasanpur, A. Ghazavizadeh, A. Sadeghi, M. Haboussi, *J. Mech. Behav. Biomed. Mater.* **2021**, *124*, 104768.
- [41] M. P. Staiger, A. M. Pietak, J. Huadmai, G. Dias, *Biomaterials* **2006**, *27*, 1728.
- [42] J. Gonzalez, R. Q. Hou, E. Nidadavolu, R. Willumeit-Römer, F. Feyerabend, *Bioact. Mater.* **2018**, *3*, 174.
- [43] D. Mei, S. V. Lamaka, X. Lu, M. L. Zheludkevich, *Corros. Sci.* **2020**, *171*, 108722.
- [44] C. Rendenbach, H. Fischer, A. Kopp, K. Schmidt-Bleek, H. Kreiker, S. Stumpp, M. Thiele, G. Duda, H. Hanken, B. Beck-Broichsitter, O. Jung, N. Kröger, R. Smeets, M. Heiland, *Mater. Sci. Eng. C.* **2021**, *129*, 112380.
- [45] W. Ali, M. Echeverry-Rendón, G. Dominguez, van K. Gaalen, A. Kopp, C. González, J. Llorca, *Biomater. Adv.* **2023**, *147*, 213325.
- [46] S.-W. Hwang, H. Tao, D.-H. Kim, H. Cheng, J.-K. Song, E. Rill, M. A. Brenckle, B. Panilaitis, S. M. Won, Y.-S. Kim, Y. M. Song, K. J. Yu, A. Ameen, R. Li, Y. Su, M. Yang, D. L. Kaplan, M. R. Zakin, M. J. Slepian, Y. Huang, F. G. Omenetto, J. A. Rogers, *Science* **2012**, *337*, 1640.
- [47] J.-Y. Bae, E.-J. Gwak, G.-S. Hwang, H. W. Hwang, D.-J. Lee, J.-S. Lee, Y.-C. Joo, J.-Y. Sun, S. H. Jun, M.-R. Ok, J.-Y. Kim, S.-K. Kang, *Adv. Sci.* **2021**, *8*, 2004029.
- [48] E. J. Curry, K. Ke, M. T. Chorsi, K. S. Wrobel, A. N. Miller, A. Patel, I. Kim, J. Feng, L. Yue, Q. Wu, C.-L. Kuo, K. W.-H. Lo, C. T. Laurencin, H. Ilies, P. K. Purohit, T. D. Nguyen, *Proc. Natl. Acad. Sci.* **2018**, *115*, 909.
- [49] R. Li, S. Xie, L. Zhang, L. Li, D. Kong, Q. Wang, R. Xin, X. Sheng, L. Yin, C. Yu, Z. Yu, X. Wang, L. Gao, *Nano Res.* **2018**, *11*, 4390.
- [50] S.-W. Hwang, J.-K. Song, X. Huang, H. Cheng, S.-K. Kang, B. H. Kim, J.-H. Kim, S. Yu, Y. Huang, J. A. Rogers, *Adv. Mater.* **2014**, *26*, 3905.
- [51] M. Ben-David, I. Carmeli, R. Orgad, B. Nathansohn-Levi, T. Yered, E. Shor, N. Wasserberg, *J. Surg. Res.* **2022**, *278*, 49.
- [52] J. Li, A. Khalid, R. Verma, A. Abraham, F. Qazi, X. Dong, G. Liang, S. Tomljenovic-Hanic, *Nanomaterials* **2021**, *11*, 695.
- [53] C. Dagdeviren, S.-W. Hwang, Y. Su, S. Kim, H. Cheng, O. Gur, R. Haney, F. G. Omenetto, Y. Huang, J. A. Rogers, *Small* **2013**, *9*, 3398.
- [54] *Synthetic Biodegradable Polymers* (Eds: B. Rieger, A. Künkel, G. W. Coates, R. Reichardt, E. Dinjus, T. A. Zevaco), Springer Berlin Heidelberg, Berlin, Heidelberg **2012**.

- [55] K. O. Siegenthaler, A. Künkel, G. Skupin, M. Yamamoto, *Synthetic Biodegradable Polymers*, Springer Berlin Heidelberg, Berlin, Heidelberg **2012**, p. 91.
- [56] Y.-W. Wang, W. Mo, H. Yao, Q. Wu, J. Chen, G.-Q. Chen, *Polym. Degrad. Stab.* **2004**, *85*, 815.
- [57] A. Wang, Y. Gan, H. Yu, Y. Liu, M. Zhang, B. Cheng, F. Wang, H. Wang, J. Yan, *J. Biomed. Mater. Res. A.* **2012**, *100A*, 1505.
- [58] A. R. Bagheri, C. Laforsch, A. Greiner, S. Agarwal, *Global Chall.* **2017**, *1*, 1700048.
- [59] N. Sinsereekul, T. Wangkam, A. Thamchaipenet, T. Sriksirin, L. Eurwilaichitr, V. Champreda, *Appl. Microbiol. Biotechnol.* **2010**, *86*, 1775.
- [60] R. Scaffaro, A. Maio, F. Sutura, E. Gulino, M. Morreale, *Polymers* **2019**, *11*, 651.
- [61] J. Karst, M. Hentschel, F. Sterl, H. Linnenbank, M. Ubl, H. Giessen, *Opt. Mater. Express* **2020**, *10*, 1346.
- [62] K. B. Das, A. N. Gerritsen, *J. Appl. Phys.* **1962**, *33*, 3301.
- [63] P. W. Bridgman, *Proc. Am. Acad. Arts Sci.* **1932**, *67*, 29.
- [64] P. Rénucci, L. Gaudart, J. P. Pétrakian, D. Roux, *Thin Solid Films* **1985**, *123*, 281.
- [65] H. Guo, S. Liu, L. Huang, D. Wang, Y. Du, M. Chu, *Metals* **2021**, *11*, 554.
- [66] S. Li, D. Yu, H. Ji, B. Zhao, L. Ji, X. Leng, *Biomed. Eng. Online.* **2018**, *17*, 87.

How to cite this article: K. A. Janus, S. Achtsnicht, A. Drinic, A. Kopp, M. Keusgen, M. J. Schöning, *Appl. Res.* **2023**, e202300102. <https://doi.org/10.1002/appl.202300102>